Embedded Function Approach for Turbulent Flow Prediction

J. D. A. Walker* and M. C. Ece†
Lehigh University, Bethlehem, Pennsylvania 18015
and
M. J. Werle‡
United Technologies Research Center, East Hartford, Connecticut 06101

In conventional prediction methods for the influence of turbulent flow on surface properties, very small mesh sizes and considerable computational effort are required to adequately resolve the intense velocity and temperature profile variations that occur in the wall layer. In this study, an approach is described wherein an outer region numerical solution is smoothly matched to a set of embedded analytic profile functions in the near-wall region; these profile functions have been derived through consideration of the coherent structure of the time-dependent near-wall flow to provide analytic expressions for the mean velocity and enthalpy profiles in the wall layer. The concept is demonstrated through example applications to turbulent boundary-layer flows in two dimensions. The technique is shown to be very efficient, and it is demonstrated that a reduction of approximately half the mesh points across the layer may be realized (as compared to conventional methods) with no degradation in accuracy.

Nomenclature

B_i = wall layer "log-law" constant for total enthalpy
B_o = outer region "log-law" parameter for total enthalpy
C_f = skin friction coefficient, $2u_\tau^2/U_e^2$
C_p^* = specific heat at constant pressure
C_i = inner wall-layer "log-law" constant for velocity
C_o = outer "log-law" parameter for velocity
F = scaled velocity, u/U_e
H = dimensionless total enthalpy, Eq. (1)
I = total enthalpy ratio, H/H_e
I_w = total enthalpy ratio at wall, H_w/H_e
K = outer region eddy viscosity constant, Eq. (28)
K_h = outer region eddy conductivity constant, Eq. (31)
L_{ref}^* = representative length
M_e = mainstream Mach number
n = normal coordinate
Pr = Prandtl number
p = pressure
q_* = dimensionless heat flux, Eq. (16)
Re_{ref} = Reynolds number
r = dimensionless radius of revolution
St = Stanton number, Eq. (18)
s = streamwise coordinate
T = dimensionless temperature
T_B^+ = wall-layer burst period
U_e = dimensionless mainstream velocity
U_{ref}^* = representative flow speed
U^+ = wall-layer velocity profile function
u = streamwise velocity
u_* = scaled friction velocity, u_τ/U_e
u_τ = dimensionless friction velocity
V = quantity defined by Eq. (6b)
v = transverse velocity
Y^+ = scaled wall-layer normal coordinate
β_c = Clauser pressure gradient parameter, Eq. (34)
γ = specific heat ratio
δ^* = dimensionless displacement thickness
Δ = outer region normal scale, Eqs. (4) and (36)
ξ,η = scaled independent variables, Eq. (4)
ϵ,ϵ_H = eddy viscosity and conductivity coefficients
κ = von Kármán constant (0.41)
κ_θ = inverse slope of the total enthalpy profile
ρ = density
μ = viscosity
θ^+ = wall-layer enthalpy profile function

Subscripts

ref = reference quantities
e = mainstream quantities
w = quantities evaluated at the wall

Received May 11, 1987; presented as Paper 87-1464 at the AIAA 19th Fluid Dynamics Conference, Honolulu, HI, June 8–10, 1987; revision received Aug. 13, 1990; accepted for publication Sept. 14, 1990.

*Professor, Department of Mechanical Engineering and Mechanics. Member AIAA.

†Graduate Research Assistant, Department of Mechanical Engineering and Mechanics.

‡Director, Technology Resources. Associate Fellow AIAA.

I. Introduction

In the numerical computation of turbulent flows, a substantial number of the total mesh points and a significant amount of iterative computational effort are required to adequately resolve the relatively intense temperature and velocity profile variations that occur near solid walls. In a typical viscous flow prediction method, which attempts to compute the mean flow all the way to the wall, on the order of 50% or more of the total mesh points will be used in the wall-layer region; here the term "wall layer" is understood to denote the portion of the flowfield ranging from the wall itself (at $y = 0$) to locations in the flow where the mean velocity and temperature profiles are effectively logarithmic in normal distance y from the wall. In most circumstances, the turbulent mean flowfield is double-structured; for external flows, the mean structure consists of an outer inviscid region and a relatively thin wall layer,[1-3] whereas for internal flows, the structure consists of an effectively inviscid core flow[1] and a thin wall layer. In this study, an efficient and accurate scheme to model and compute the mean flow and temperature fields in the wall layer is described.

It is well known that the equations governing the mean flow in the outer region of an attached viscous flow (or the core region of an internal flow) may be reasonably well-represented using relatively simple turbulence models. For example, in the

model of Mellor and Gibson,[4] the eddy viscosity function is initially linear in y (in order that the mean profile near the wall be logarithmic) and at a specific value of y becomes constant throughout most of the outer region. This model forms the basis for the outer region model for a number of modern turbulence prediction methods.[5,6] To satisfy the no slip condition at the wall, it is necessary to introduce an inner region model for the wall layer, and the conventional approach[5] is to modify the linear eddy viscosity near the wall by multiplying by the Van Driest damping function. This function originates in an analysis of the time-dependent flow in the wall layer carried out over 30 years ago by Van Driest[7]; unfortunately, modern experimental studies[8-10] show that the physical picture of the wall-layer flow that forms the basis of the Van Driest model is fallacious. Nevertheless, a variety of ad hoc corrections and correlations have been appended[5] to the Van Driest damping function over the years to account for various effects, such as pressure gradients and wall blowing. One objective of the present study was to develop an approach to replace such inner region models using rational mechanics concepts.

The present methodology may be described as an embedded function (EF) method in which the mean velocity and enthalpy profiles in the wall layer are represented by analytical functions directly embedded into the finite difference representation of the flow. These inner region profiles are based upon consideration of the experimentally observed coherent structure of the time-dependent wall-layer flow.[8-12] In the approach described here, an outer layer numerical solution is continually matched along the entire surface to the analytical wall-layer profiles.

It is worthwhile to note that the present method bears an apparent but superficial similarity to the early wall-function methods described by Launder and Spalding.[13] Because of the obvious mesh and computation economies that can accrue with such an approach, there has been considerable interest in developing computational algorithms for turbulent flows that incorporate wall-function concepts.[14-16] In the conventional wall-function approach,[14-16] an outer layer numerical solution is patched to an inner logarithmic "law of the wall" at the first mesh point off the wall; the wall-layer profile is generally formed by patching an extension of the logarithmic law deep into the wall layer onto an assumed linear velocity profile close to the wall. The present method is significantly different in application and background from current wall-function methods. First, the outer region numerical solution is matched to an analytical wall-layer profile, which smoothly spans the entire distance from the logarithmic region to the wall. Second, the joining of the outer layer numerical solution and wall-layer analytical profiles is accomplished through smooth asymptotic matching (vs patching); skin friction and heat transfer coefficients are obtained from algebraic relations that arise from the analysis and that ensure a proper matching (in the asymptotic sense) between the outer region numerical solutions and the analytical wall-layer models. Third, the smooth joining of the outer region numerical solution to the rapidly varying wall-layer velocity near the surface involves some subtle but important aspects that are not addressed in conventional wall-function methods (which may account for the difficulties experienced by some authors using wall functions). A crucial feature of the present technique is that a scaled normal variable is introduced to ensure a smooth matching of the outer layer numerical solution and the wall-layer functionals as the calculation proceeds downstream; this aspect will be discussed in detail subsequently. It should be noted that the present method is in a similar spirit to another recent scheme[17] in which a "law of the wake" formula was adopted close to the surface; in a numerical solution for the flow in the outer region, the first mesh point off the wall was taken well above the overlap zone between the inner and outer layer. In contrast, the present methodology carries out the match in the overlap zone to the embedded functions, which then span the remaining distance to the wall.

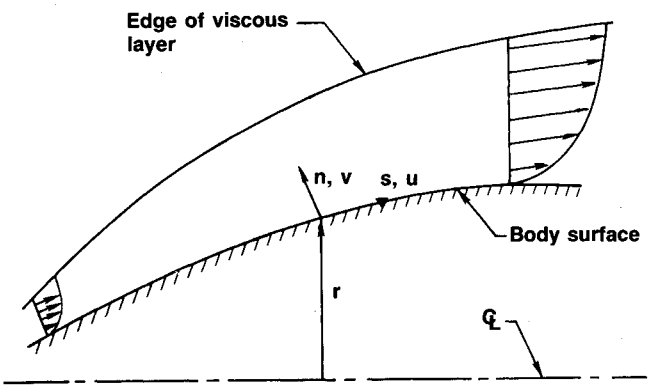

Fig. 1 Coordinate system.

The plan of the paper is as follows. In Sec. II, the governing equations are described and the problem is formulated. The asymptotic behavior of the outer region solution near the wall is discussed in Sec. III. The simple outer region turbulence models used in this study are given in Sec. IV; note that the methodology can readily be applied to more complicated outer region models and the simple models used here are primarily for demonstration purposes. An outer layer scaling function, which ensures that the outer region numerical solution matches the wall-layer profiles at a constant value of Y^+ as the calculation proceeds downstream, is discussed in Sec. V. The numerical methods associated with the treatment of the asymptotic boundary conditions near the wall are described in Sec. VI, and sample calculated results are given in Sec. VIII.

II. Formulation

Consider a two-dimensional attached viscous flow on either a planar surface or a body of revolution; the coordinate system used is orthogonal and associated with the contour of the wall, as indicated in Fig. 1.

Here s and n measure distances in the directions tangential and normal to the body surface, respectively, and u, v, are the corresponding velocity components. In addition, r is the dimensionless radius of revolution for an axisymmetric body, with $r = 1$ for a two-dimensional planar flow. In the equations that follow, all lengths and velocities have been made dimensionless with respect to L^*_{ref} and U^*_{ref}, a representative length and flow speed, respectively; the density and absolute viscosity are made dimensionless with respect to reference quantities ρ^*_{ref} and μ^*_{ref}, respectively. Throughout the paper an asterisk superscript denotes a dimensional quantity. The dimensionless total enthalpy (with respect to U^{*2}_{ref}) is given by

$$H = T + u^2/2 \tag{1}$$

where T is dimensionless temperature (with respect to $U^{*2}_{\text{ref}}/C^*_p$, where C^*_p is the specific heat at constant pressure). The reference Reynolds number and Prandtl number are defined by

$$Re_{\text{ref}} = \rho^*_{\text{ref}} U^*_{\text{ref}} L^*_{\text{ref}}/\mu^*_{\text{ref}} \tag{2a}$$

$$Pr = \mu^* C^*_p/k^* \tag{2b}$$

where k^* is the thermal conductivity. The ideal gas law

$$p = (\gamma - 1)\rho T/\gamma \tag{3}$$

is used as the equation of state, where $\gamma = C^*_p/C^*_v$ is the ratio of specific heats; the viscosity μ is computed at any location as a function of T alone from the Sutherland relation.[6]

The present method applies to situations where the flow near the wall is fully turbulent, and the transformations described here are tailored specifically to this situation. A new set of

normalized coordinates are defined by

$$\xi = \int_0^s \rho_e \mu_e U_e r^2 \, ds, \qquad \eta = \frac{U_e r Y}{\Delta} \tag{4}$$

where Y is the Howarth-Dorodnitsyn variable

$$Y = \int_0^n \rho \, dn \tag{5}$$

Here a subscript e denotes a quantity evaluated at the boundary-layer edge. The transverse coordinate η is defined in terms of a function $\Delta(\xi)$, which is proportional to the local boundary-layer thickness; the proper selection of this function is important to the success of the method and a specific choice for Δ will be described subsequently in Sec. V. Normalized dependent variables are defined according to

$$F = u/U_e, \qquad I = H/H_e \tag{6a}$$

$$V = \frac{1}{\rho_e \mu U_e r^2}\left\{\frac{r\rho v}{\Delta} + \left.\frac{\partial \eta}{\partial s}\right|_n F\right\} \tag{6b}$$

and for the outer region, a dimensionless eddy viscosity coefficient ϵ and eddy conductivity coefficient ϵ_H are defined by

$$-\overline{u'v'} = \epsilon \frac{\partial u}{\partial n}, \qquad -\overline{v'H'} = \epsilon_H \frac{\partial H}{\partial n} \tag{7}$$

It should be noted that this choice of turbulence model is not central to the theme of this paper and is adopted here as a convenient and simple selection.

It is easily shown[18] that the two-dimensional compressible boundary-layer equations become

$$\frac{\Delta'}{\Delta} F + \frac{\partial F}{\partial \xi} + \frac{\partial V}{\partial \eta} = 0 \tag{8}$$

$$F\frac{\partial F}{\partial \xi} + V\frac{\partial F}{\partial \eta} = \beta(I - F^2) + \frac{\partial}{\partial \eta}\left(\bar{\mu}\frac{\partial F}{\partial \eta}\right) \tag{9}$$

$$F\frac{\partial I}{\partial \xi} + V\frac{\partial I}{\partial \eta} = \alpha\frac{\partial}{\partial \eta}\left[\hat{\mu}\frac{\partial}{\partial \eta}\left(\frac{F^2}{2}\right)\right] + \frac{\partial}{\partial \eta}\left(\bar{k}\frac{\partial I}{\partial \eta}\right) \tag{10}$$

in which the following definitions have been used:

$$\beta = \frac{1}{M_e}\frac{dM_e}{d\xi} \tag{11a}$$

$$\alpha = \frac{(\gamma-1)M_e^2}{1+[(\gamma-1)/2]M_e^2} \tag{11b}$$

$$\hat{\mu} = \frac{\rho\mu}{\rho_e\mu_e\Delta^2}\left(1 - \frac{1}{Pr}\right)\frac{1}{Re_{\text{ref}}} \tag{11c}$$

$$\bar{\mu} = \frac{\rho\mu}{\rho_e\mu_e\Delta^2}\left(\frac{1}{Re_{\text{ref}}} + \frac{\rho\epsilon}{\mu}\right) \tag{11d}$$

$$\bar{k} = \frac{\rho\mu}{\rho_e\mu_e\Delta^2}\left(\frac{1}{Re_{\text{ref}}Pr} + \frac{\rho\epsilon_H}{\mu}\right) \tag{11e}$$

Here, M_e denotes the local mainstream Mach number, and the prime in Eq. (8) denotes differentiation with respect to ξ. These equations are to be solved subject to the conditions

$$I, F \to 1 \quad \text{as} \quad \eta \to \infty \tag{12}$$

at the boundary-layer edge.

In a conventional boundary-layer prediction method,[5-6] a turbulence-model distribution is assumed for both the outer region and the wall layer; the velocity and enthalpy profiles are then computed all the way to the wall, subject to the additional boundary conditions $F = V = 0$, $I = I_w = H_w/H_e$ at $Y = 0$. In the present method, the numerical calculation is carried out only in the outer region of the boundary layer and matched onto a set of inner region profiles spanning the wall layer; these wall-layer profiles are functions of the scaled inner variable

$$Y^+ = Re_{\text{ref}} U_e u_* Y/\mu_w \tag{13}$$

where u_* is the ratio of local skin friction to mainstream velocities defined by

$$u_* = \frac{u_\tau}{U_e}, \qquad u_\tau^2 = \frac{\mu_w}{\rho_w Re_{\text{ref}}}\left.\frac{\partial u}{\partial n}\right|_{n=0} \tag{14}$$

Here, a subscript w indicates that a quantity is evaluated at the wall. Note that the inner variable in Eq. (13) is defined in terms of the Howarth-Dorodnitsyn variable but, for small n (near the surface), is equivalent to the conventional (incompressible) definition of the wall layer coordinate $y^+ = L^*_{\text{ref}} u^*_\tau n/\nu^*_w$, where an asterisk denotes a dimensional quantity. A general asymptotic analysis[10,18] shows that leading order velocity and enthalpy distributions in the wall layer are of the form

$$F = u_* U^+(Y^+) + \cdots \tag{15a}$$

$$I = I_w + q_* \theta^+\left(Y^+\sqrt{Pr}\right) + \cdots \tag{15b}$$

where

$$I_w = \frac{H_w}{H_e}, \qquad q_* = \frac{q_w}{\rho_w u_\tau H_e} \tag{16}$$

and q_w is the local dimensionless heat flux from *fluid to wall,* defined by

$$q_w = \frac{k^*}{\rho^*_{\text{ref}} U^{*3}_{\text{ref}}}\left.\frac{\partial T^*}{\partial n^*}\right|_{n^*=0} \tag{17}$$

Again, asterisks denote dimensional quantities. Note that it is possible to express the dimensionless heat flux q_* in terms of a Stanton number in the following manner:

$$St = \frac{q_w}{\rho_w U_e (H_e - H_w)} = \frac{q_* u_*}{1 - I_w} \tag{18}$$

The profile functions U^+ and θ^+ have the following general asymptotic forms[18-20]:

$$U^+ \sim \frac{1}{\kappa}\log Y^+ + C_i \tag{19a}$$

$$\theta^+ \sim \frac{1}{\kappa_\theta}\log\left(Y^+\sqrt{Pr}\right) + B_i \tag{19b}$$

as $Y^+ \to \infty$ at the outer edge of the wall layer. Here, κ is the von Kármán constant and κ_θ is the analogous quantity for the total enthalpy distribution; C_i and B_i are constants. The specific inner region profile models, as well as how κ_θ, B_i, C_i are determined, will be discussed in Sec. IV.

III. Asymptotic Behavior Near the Wall

In the outer region of the viscous layer, the velocity and enthalpy distributions may be written in the form of a defect law according to

$$F = 1 + u_* U_1(\xi,\eta) + \cdots \tag{20a}$$

$$I = 1 + q_* \Theta_1(\xi,\eta) + \cdots \tag{20b}$$

where $I_w = H_w/H_e$. Here, U_1 and Θ_1 are defect functions of the outer variable η, defined in Eq. (4); a general asymptotic

analysis[19,20] shows that both functions must be logarithmic, as $\eta \to 0$ in order to match the wall-layer profiles near the wall, whose limiting form is given by Eqs. (19). Note that there are some changes in the notation and scalings in this paper from Ref. 18, which now reflect a more general approach.[20] The general form of F and I near the wall is independent of turbulence model[19,20] and is given by

$$F \sim 1 + u_* \left\{ \frac{1}{\kappa} \log\eta + C_o \right\}, \quad \text{as } \eta \to 0 \tag{21a}$$

$$I \sim 1 + q_* \left\{ \frac{1}{\kappa_\theta} \log\eta + B_o \right\}, \quad \text{as } \eta \to 0 \tag{21b}$$

Here B_o and C_o are generally functions of the streamwise variable ξ that depend implicitly on the turbulence model and that are generally determined in the course of the calculations. The variable V is related to the transverse velocity v through Eq. (6b), and it is easily shown from Eq. (8) [as well as the velocity match condition (23a)] that in general

$$V \sim -\left\{ \frac{\Delta'}{\Delta} + \frac{u_*'}{u_*} \right\} \eta F + \frac{u_* \eta}{\kappa} \left\{ \frac{r'}{r} + \frac{\mu_w'}{\mu_w} \right\}, \quad \text{as } \eta \to 0 \tag{22}$$

In this equation, F is understood to have the asymptotic form indicated by Eq. (21a), and the primes denote differentiation with respect to ξ; in addition, the inner region log-law parameter C_i [c.f., Eq. (19a)] is assumed constant. Note that Eq. (22) applies for a solid wall and that a modificaiton of the theory would be required for walls with transpiration.

In the present method, the numerical solution of Eqs. (8–10) was obtained subject to the boundary conditions (12) and the asymptotic conditions (21) and (22), as $\eta \to 0$. In order to obtain a smooth match to the wall-layer profile functions, two algebraic relations, which will be referred to as the "match conditions," must be satisfied. The match condition for the velocity and enthalpy profiles follow from comparison of Eqs. (15), (19), and (21), and these are

$$\frac{1}{u_*} = \frac{1}{\kappa} \log\left(Re_{\text{ref}} \frac{u_* \Delta}{r \mu_w} \right) + C_i - C_o \tag{23a}$$

$$\frac{1 - I_w}{q_*} = \frac{1}{\kappa_\theta} \log\left(Re_{\text{ref}} \sqrt{Pr} \frac{u_* \Delta}{r \mu_w} \right) + B_i - B_o \tag{23b}$$

These important relations connect q_* and u_* to the characteristic parameters of the velocity and enthalpy profiles and are subsequently used to determine the local skin friction and heat transfer coefficients.

IV. Turbulence Models

It is, in general, necessary to specify a turbulence model for both the wall layer and the outer regions of the boundary layer. Asymptotic theory[1,2,20] shows that, in the limit of large Re_{ref}, the convection terms in the streamwise momentum equation are negligible to leading order in the wall layer, and the mean flow is determined through a balance of the viscous and Reynolds stresses. Consequently, it is possible to model either the Reynolds stress or the mean profile for the wall layer; the remaining unknown quantity may then be determined by integration from the wall. In recent studies,[10–12] the extensive experimental studies of the dynamics of the time-dependent flow in the wall layer of a turbulent boundary layer have been reviewed. It emerges that the main contributions to Reynolds stress and turbulent heat flux occur in the turbulence during brief periods when the wall layer interacts strongly with the outer flow. Such discrete events are extremely difficult to model, and Walker et al.[10] argue that an alternative approach is to model the contributions to the mean profiles that occur continuously as the turbulent flow in the wall layer evolves in time. In the model described by Walker et al.,[9,10] the observed coherent structure and cyclic behavior of the wall-layer flow are considered and the leading order equations describing the time-dependent wall-layer flow are obtained; possible time-dependent solutions of these equations are investigated, and these solutions are then time-averaged over a typical cycle to produce analytical models for the mean wall-layer profiles U^+ and θ^+. These profiles are analytical expressions that satisfy Eqs. (19), as $Y^+ \to \infty$ and the compatibility conditions[9,10]

$$\frac{\partial U^+}{\partial Y^+} = 1, \quad \frac{\partial^2 U^+}{\partial Y^{+2}} = \frac{\partial^3 U^+}{\partial Y^{+3}} = 0 \quad \text{at } Y^+ = 0 \tag{24}$$

$$\frac{\partial \theta^+}{\partial Y^+} = Pr, \quad \frac{\partial^2 \theta^+}{\partial Y^{+2}} = \frac{\partial^3 \theta^+}{\partial Y^{+3}} = 0 \quad \text{at } Y^+ = 0 \tag{25}$$

at the wall. The profiles have the functional form

$$U^+ = U^+(Y^+, \kappa, T_B^+), \quad \theta^+ = \theta^+(Y^+\sqrt{Pr}, \kappa_\theta, T_B^+) \tag{26}$$

where T_B^+ is the mean period between bursts in the wall layer.[10] In this study, universal values of $\kappa = 0.41$ for the von Kármán constant and $T_B^+ = 110.2$ for the burst period were assumed; note that these values yield the commonly accepted value of the wall-layer log-law constant $C_i = 5.0$, and further that the assumed value of T_B^+ is consistent with direct experimental measurements of this quantity.[10] The heat transfer problem is complicated by the fact that κ_θ is not a universal constant, and careful comparison[19] with experimental data show that κ_θ depends on local flow conditions. The following relations have been obtained from asymptotic theory[19,20] and express κ_θ in terms of either St or q_*:

$$\kappa_\theta = \kappa \frac{St}{u_*^2} = \frac{\kappa}{1 - I_w} \frac{q_*}{u_*} \tag{27}$$

This relation, as well as $T_B^+ = 110.2$, was used in the present study; thus, B_i and the wall-layer profile θ^+ may be completely determined.[20] Both wall-layer profiles are summarized in the Appendix.

With the wall-layer velocity and enthalpy profiles known, it is only necessary in the present approach to adopt a turbulence model for the outer region of the boundary layer. The following simple model was adopted for the eddy viscosity in Eq. (7):

$$\epsilon = \frac{\rho_e \rho_w}{\rho^2} U_e \delta^* K \begin{cases} 1, & \eta \geq \eta_m \\ \eta/\eta_m, & \eta < \eta_m \end{cases} \tag{28}$$

where

$$\eta_m = \frac{r \rho_e U_e \delta^*}{\Delta u_*} \left(\frac{K}{\kappa} \right), \qquad K = 0.0168 \tag{29}$$

$\kappa = 0.41$ is the von Kármán constant and δ^* is the dimensionless (incompressible) thickness, defined by

$$\delta^* = \int_0^\infty (1 - F)\, dn \tag{30}$$

This type of outer region model is fairly common.[4,6] The linear dependence in Eq. (28) for small η is necessary to obtain a logarithmic behavior in F; on the other hand, the assumed constant behavior for large η yields the proper exponential decay in F, as $\eta \to \infty$. The simplest model meeting these requirements is the "ramp" formula defined in Eq. (28), with the patch point at η_m defined as a function of ξ by Eq. (29). A further point is related to the density factors introduced in Eq. (28). It is usually assumed[5,6] that turbulence models that have been developed for incompressible flow can be extended without modification to the high-speed compressible regime. However, a recent study[20] shows that this procedure can give inconsistent results; the model in Eq. (28) is self-consistent at high Mach numbers[20] and reduces to the essential features of the Cebeci-Smith model[5] in the limit of low Mach numbers.

A similar model was adopted for the eddy conductivity function in Eq. (7) according to

$$\epsilon_H = \frac{\rho_e \rho_w}{\rho^2} U_e \delta^* K_h \begin{cases} 1, & \eta \geq \tilde{\eta}_m \\ \eta/\tilde{\eta}_m, & \eta < \tilde{\eta}_m \end{cases} \tag{31}$$

where

$$\tilde{\eta}_m = \frac{r \rho_e U_e \delta^*}{\Delta u_*} \left(\frac{K_h}{\kappa_\theta} \right) \tag{32}$$

The local variation of κ_θ is described by Eq. (27). In addition, it has also been determined[19] that K_h exhibits a small but significant dependence on pressure gradient; the following correlation[19] for K_h was used.

$$K_h = \begin{cases} 0.0245 - 0.00276\beta_c, & \beta_c \leq 2 \\ 0.0190, & \beta_c > 2 \end{cases} \tag{33}$$

where β_c is the Clauser pressure gradient parameter defined (in the present variables) by

$$\beta_c = \frac{L^*_{\text{ref}} \delta^* \, dp_e^*/dx^*}{\tau_w^*} = -\frac{\rho_e^2 \mu_e \delta^* r^2}{\rho_w u_*^2} \frac{dU_e}{d\xi} \tag{34}$$

It should be noted that this model for the turbulent heat flux term has been developed independent of any type of Reynolds analogy argument; the model has been shown to yield excellent heat transfer predictions[19] in range $-0.6 < \beta_c < 2.0$ where reliable data are available. For strong adverse pressure gradients ($\beta_c > 2.0$), where it has not been possible to test the model against data, a constant value of K_h was used in Eq. (31). It should be noted that the outer region turbulence models (28) and (31) have been modified from those given in Ref. 18 to reflect recent work[20] associated with supersonic turbulent boundary layers. For low Mach number flows, the present models become essentially the same as the models used in Ref. 18.

V. Outer Scale

To completely define the prediction algorithm, it remains to discuss the selection of the outer region scale Δ, introduced in Eq. (4). For each value of η there is a corresponding value of Y^+, and using Eqs. (4) and (13), it may be seen that the two variables are related by

$$Y^+ = Re_{\text{ref}} u_* \eta \Delta / r \mu_w \tag{35}$$

In the (ξ,η) coordinate system, the calculation of the solution of Eqs. (8–10), proceeds downstream along lines of fixed η, starting from some initial ξ station. Denote the mesh line closest to the wall by $\eta = \eta_2$ (see Fig. 2) and assume that this is where the match to the wall-layer profile functions is to be made.

In principle, many choices are possible for Δ, subject to the requirement[19,20] that Δ is $O(u_*)$; however, if Y_m^+ denotes the value of Y^+ corresponding to $\eta = \eta_2$ at the initial ξ station, the values of Y^+ corresponding to η_2 at successive stations downstream will in general differ from Y_m^+. It is possible to guarantee that the match point at $\eta = \eta_2$ corresponds to a fixed value of Y^+ at all downstream locations by selecting Δ according to

$$\Delta = r \mu_w Y_m^+ / (\eta_2 u_* Re_{\text{ref}}) \tag{36}$$

A typical value of Y_m^+ used was $Y_m^+ = 60$ and, as the calculation proceeds downstream, $\Delta(\xi)$ is determined at each streamwise location from Eq. (36). It is worthwhile to note that for the choice of Δ, the asymptotic form of V near the wall in Eq. (22) becomes

$$V \sim \eta \left\{ \frac{r'}{r} + \frac{\mu_w'}{\mu_w} \right\} \left\{ \frac{u_*}{\kappa} - F \right\} \quad \text{as } \eta \to 0 \tag{37}$$

Here again F denotes the asymptotic form given in Eq. (21a), and the primes denote differentiation with respect to ξ.

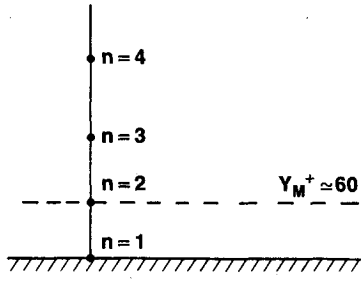

Fig. 2 Mesh numbering system near the wall.

VI. Numerical Methods

The numerical method used to advance the solution of Eqs. (8–10) from an initial ξ station is described in detail in Ref. 18. It is a first-order accurate implicit marching scheme in which streamwise gradients are approximated by simple backward differences and second-order accurate differences are used for the η derivatives at the current ξ station. The boundary conditions (12) are applied at a large but finite value of η, as an approximation, as the calculation proceeds downstream. The basic numerical scheme is therefore standard[6,18] and the only novel treatment of the asymptotic boundary conditions will be considered in detail here.

The difference equations are a set of nonlinear algebraic equations. To solve these equations, it is convenient to write

$$F_n = \bar{F}_n + \delta F_n \tag{38a}$$

$$V_n = \bar{V}_n + \delta \bar{V}_n \tag{38b}$$

$$I_n = \bar{I}_n + \delta I_n \tag{38c}$$

at each internal mesh point, where $n = 2,3,\ldots,N$; the numbering system is depicted schematically in Fig. 2. In these equations, the overbar denotes a known estimate (either from the previous ξ station or the previous iteration at the current station). When Eqs. (38) are substituted into the difference equations and quadratic terms in δF_n, δV_n, or δI_n are neglected, a set of linear difference equations are obtained at any stage. These equations were solved by a generalized form of the Thomas algorithm,[18] which has back-substitution recurrence equations of the form

$$\delta F_n = A_n + B_n \delta V_{n-1} + C_n \delta F_{n-1} + D_n \delta I_n \tag{39a}$$

$$\delta I_n = \tilde{A}_n + \tilde{B}_n \delta V_{n-1} + \tilde{C}_n \delta F_{n-1} + \tilde{D}_n \delta I_n \tag{39b}$$

$$\delta V_n = A_n^* + \delta V_{n-1} + C_n^* \delta F_{n-1} + E_n^* \delta I_n \tag{39c}$$

Specific formulas for the coefficients in Eqs. (39) are given in Ref. 18.

The asymptotic conditions (21) and (37) were incorporated into the basic numerical scheme in the following way. The two mesh points η_2 and η_3 (see Fig. 2) were selected close enough to the wall so that the asymptotic forms (21) and (37) may be assumed to give a good representation of the solution; typically, the values of η_2 and η_3 were such that $Y_m^+ \simeq 60$ at $\eta = \eta_2$, and η_3 was selected a small percentage larger than the value of η_2. It follows that

$$F_3 - F_2 = \frac{u_*}{\kappa} \log\left(\frac{\eta_3}{\eta_2} \right) \tag{40}$$

$$I_3 - I_2 = \frac{q_*}{\kappa_\theta} \log\left(\frac{\eta_3}{\eta_2}\right) \tag{41}$$

Note that these relations do not contain the outer region log-law functions C_o and B_o (which are to be found at any ξ station) and, for a given estimate of u_* and q_*, may be thought of as fixing the profile slopes near the wall. The expression for V at the first mesh point from the wall is

$$V_2 = \eta_2 \left\{\frac{r'}{r} + \frac{\mu_w'}{\mu_w}\right\}\left\{\frac{u_*}{\kappa} - F_2\right\} \tag{42}$$

It is possible to write Eqs. (40–42) in the following delta forms:

$$\delta F_3 = \delta F_2 + M \tag{43a}$$

$$\delta I_3 = \delta I_2 + L \tag{43b}$$

$$\delta V_2 = J\delta F_2 + K \tag{43c}$$

where, for example,

$$M = \bar{F}_2 - \bar{F}_3 + \frac{u_*}{\kappa} \log\left(\frac{\eta_3}{\eta_2}\right) \tag{44}$$

and the overbar denotes estimates of the indicated quantity from the previous iteration. Similarly, expressions for J, K, and L are easily obtained.[18] Upon substitution of Eqs. (43) into the first two of the back substitution formulas (39) to eliminate δF_2, δI_3, and δV_2. It may be inferred that two equations for δF_2 and δI_2 are obtained[18]; the solution of these two equations was used at any stage to initiate a back substitution in Eqs. (39) to determine values of δF_n, δV_n, and δI_n across the boundary layer ($n = 3, 4, \ldots, N$).

At any given ξ station, an iterative method of solution is necessary. This was accomplished as follows. At any stage, estimates of u_* and q_* are available either from a previous iterate or, at the first iteration, from values at the previous ξ station. With these estimates, new iterates for the outer scale in Eq. (36) and the coefficients in the difference equations were computed. A solution of the difference equations was then carried out to produce new velocity and enthalpy profiles. Using the new values of F and I at $\eta = \eta_2$, revised estimates of the outer region log-law parameters C_o and B_o were obtained from Eqs. (21). Note that these quantities are functions of ξ, and are determined as the computation proceeds downstream. New estimates of the local skin friction and heat transfer were then obtained by solving the match conditions (23) for u_* and q_*, respectively. This process was continued at each ξ station until convergence occurred.

VII. Calculated Results

The Embedded Function (EF) method has been applied here to situations where the flow is fully turbulent. To start a calculation, a set of profiles at some initial station is required. These initial profiles were obtained in two ways. In the first scheme, a conventional finite-difference technique (the UTRC ABLE[6,18] code) was used to provide an initial set of profiles in the fully turbulent regime for a given geometry, as follows. A computation is initiated by solving the laminar similarity equations at a front stagnation point. The calculation then proceeds downstream, evaluating the solution of the laminar boundary-layer equations. The streamwise locations where transition starts and ends are input variables to the calculation. This computation proceeds through the streamwise extent of transition and then into the fully turbulent regime, using a Cebeci-Smith[5,6] turbulence model. In the first set of calculations described here, the ABLE code[6] provided a set of profiles at a streamwise station, $\xi = \xi_{m-1}$, for a selected location downstream of the end of the transition zone. At this station, it was convenient[1,20] to define the initial outer region scale according to $\Delta = r\rho_e U_e \delta^*/u_*$, with subsequent values in the downstream direction being determined from Eq. (36). With the η mesh defined at ξ_{m-1}, the mesh point corresponding to the closest point to $Y^+ = 60$ was designated as η_2, and all inner region mesh points for $\eta < \eta_2$ were dropped from consideration. In a typical calculation,[6] on the order of 50% of the mesh points may be eliminated in this manner. The computation was then continued downstream in the outer region using the simple models in Eqs. (28) and (31) and the wall-layer profiles. In a second set of calculations, the initial profile at ξ_{m-1} was generated independently from the ABLE code through a numerical solution of self-similar turbulent profile equations.[18]

Some examples obtained using the first method of generating initial profiles will be described here. The computed results will be compared with experimental data, as will the results predicted by the continuation of the original finite-difference solutions, using the ABLE code,[6] in order to provide a comparison with a conventional prediction method. In Fig. 3, calculated results for skin friction and Stanton number for a constant pressure flow are shown. The experimental data in Fig. 3 were obtained[21,22] for a low Mach number flow ($U^*_{\text{ref}} = 31.3$ ft/s, $T^*_e = 73.6°$F) in air. In the test section, measurements were carried out over a flat plate 8 ft long at constant surface temperature ($T_w = 98.7°$F) in air. In the experimental configuration, the flow was tripped upstream of the test section in the entrance region and, for this reason, it is not possible to completely simulate the starting conditions in the computations; in order to provide a reasonable initial condition to start the calculation, it was assumed (as input to the ABLE code[6]) that the plate extended 6 in. in the upstream direction, with transition occurring in the range from 3 to 6 in. from the leading edge. The creation of this initial condition is somewhat arbitrary, but it is evident that the calculation produces results that are consistent with the experimental data.

The important feature that should be noted from Fig. 3 is that the EF method results agree well with the predictions of the conventional method.[6,18] It may be observed in Fig. 3 that, at the switch point (which is somewhat downstream of

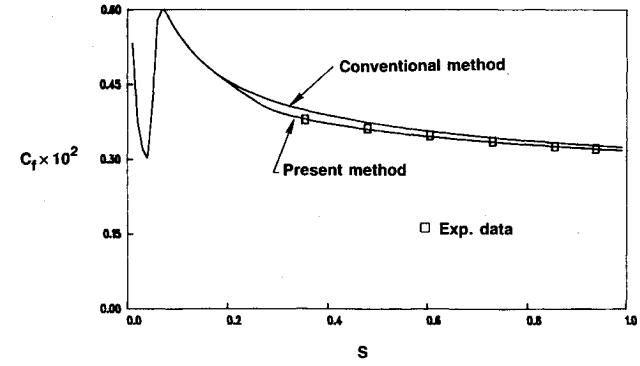

a) Skin friction

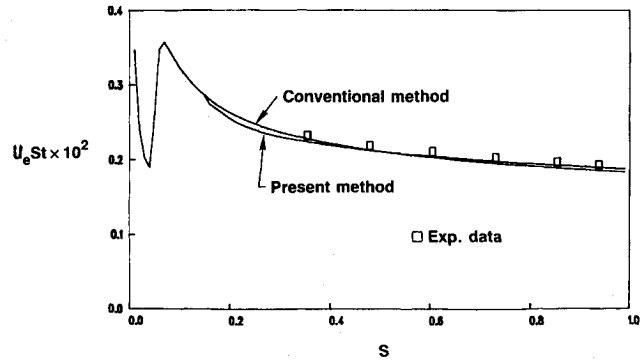

b) Heat transfer

Fig. 3 Calculated results for a flat plate boundary layer.

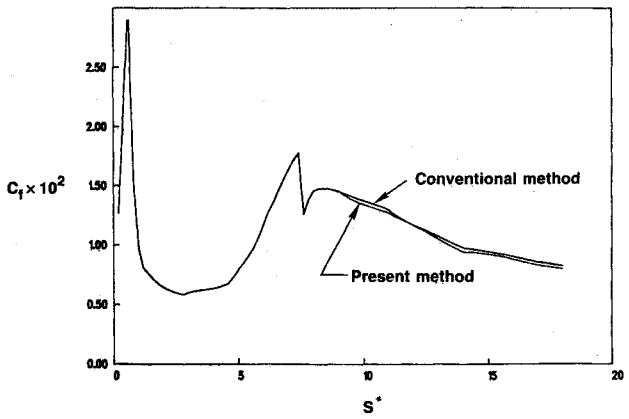

a) Skin friction

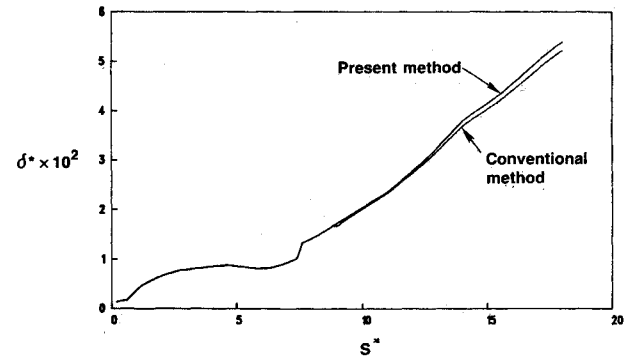

b) Displacement thickness

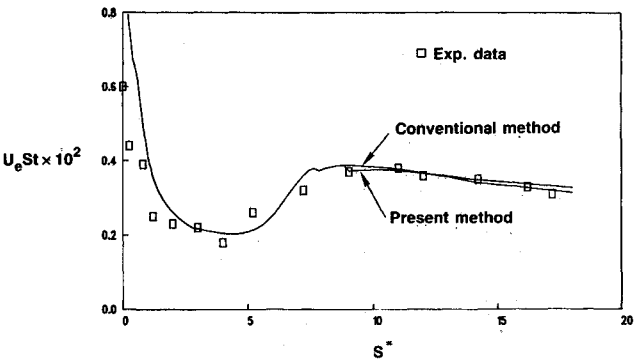

c) Heat transfer

Fig. 4 Calculated results for a heated turbine blade.

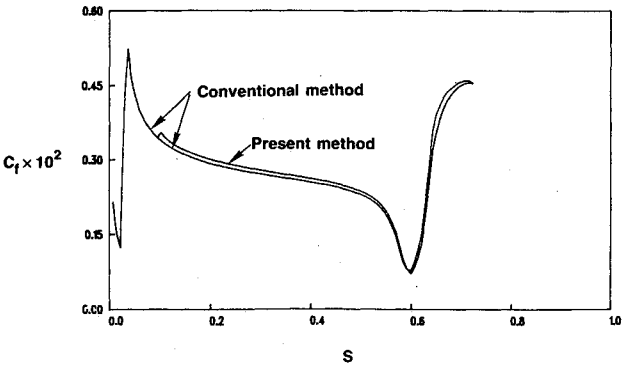

a) Skin friction

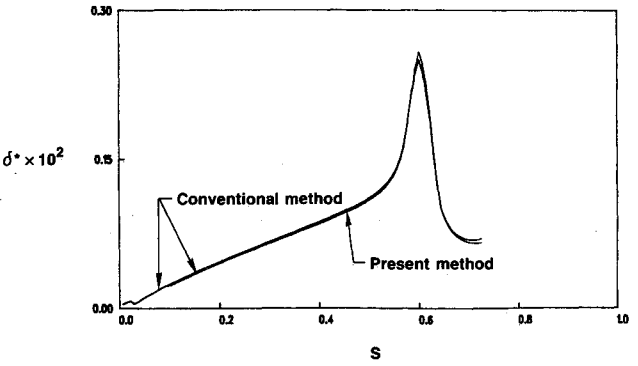

b) Displacement thickness

Fig. 5 Calculated results for axisymmetric transonic flow.

the end of the transition region near $s = 0.15$), there is a discontinuous slope in the computed quantities, as the calculation changes from the conventional method[6] to the EF formulation. These rapid initial changes are to be expected, since the problem formulation, as well as the turbulence models, change at the switch point. It may be observed, however, that the effect is not significant and that the correspondence between the results for the two approaches is quite reasonable at stations downstream.

A second example considered here corresponds to transitional flow over the suction surface of a heated turbine blade, for which experiments were carried out in air by Graziani et al.[23] The flow conditions were $p_{te}^* = 14.7$ lbf/in.^{2}, $T_{te}^* = 530$°R, and $q_w^* = 416$ Btu/hr-ft, and in the experiments transition was observed from $s^* = 3$ in. to $s^* = 8$ in. from the point of attachment on the suction surface. Calculations in this case were carried out with a variable mesh in the η direction (with 101 points across the boundary layer, as in Ref. 6) and 100 mesh points uniformly distributed in the streamwise direction; at the location where the calculation was switched to the EF method, the number of mesh points was reduced to 50 (across the outer layer). The results are plotted in Fig. 4 and again the EF computed values for skin friction, displacement thickness, and Stanton number show good agreement with continuation of the conventional procedure, as well as with the experimental data.

The third example considered here corresponds to transonic turbulent flow along a cylindrical body, which thickens into an axisymmetric bump.[6,24] The flow conditions in the analysis are $M_e = 0.85$, $p_{te}^* = 14.7$ lbf/in.^{2}, $T_{te}^* = 519$°R and the wall was assumed to be adiabatic. Calculations were initiated from a solution of the laminar compressible similarity equations for an axisymmetric body with a cone angle of 0 deg and with a nonuniform mesh with 101 points across the boundary layer.[6] There were 100 points uniformly distributed in the streamwise direction, and, at the switch to the EF method, the number of mesh points in the normal direction was reduced to 50. In this example, the flow speeds are transonic and a shock wave develops near the top of the bump. Calculations were carried out until just upstream of the shock wave. Computed results for skin friction and displacement thickness are plotted in Fig. 5, where it may be observed that good agreement with the conventional method[6] is again obtained.

A second means of initiating the boundary-layer integration was also considered,[18] in which the initial velocity and enthalpy profiles in the fully turbulent regime were obtained in a manner independent of the ABLE code. In this method, the profiles at a given streamwise location were represented as a member of a one-parameter family of turbulent similarity profiles; the method is described in Ref. 18. Computed results[18] using this method for starting the boundary-layer integrations also show very good agreement with measured data.

VIII. Conclusions

In this study, the EF method for the prediction of turbulent flows near walls has been shown to be effective. In the technique, a numerical solution of the outer region equations is

continually matched to a set of analytical profiles in the wall layer as the calculations proceeds downstream. There are several advantages to this methodology. First, a reduction on the order of 50% of the total numerical mesh points may be realized, as compared to prediction methods that seek to compute the flow all the way to the wall through the extremely high gradient regions. Second, the algorithm is very efficient since the numerical computations are carried out using very simple outer region turbulence models and complicated inner region turbulence models are not needed. Finally, skin friction and heat transfer coefficients are determined at any stage from algebraic relations, which are the mathematical statements that the outer region numerical solutions should join smoothly to the wall-layer profiles; consequently, there is no need to numerically differentiate the profiles to compute such quantities.

The methods described in this paper may be easily extended to treat more complicated surface conditions (such as wall blowing) for two-dimensional external flows. Internal flows are also double-structured, and since the wall-layer structure is very similar to boundary-layer flows, an extension to two-dimensional internal flows is easily accomplished. Recently the present approach has been extended for attached three-dimensional flows.[25] In principle, the technique could also be adopted as a boundary condition for full Navier-Stokes solutions in regions where the flow is turbulent and attached; these types of applications are currently under consideration. It is likely that the methodology may have its most significant application in three-dimensional flows, because of the substantial economies in mesh points that may be achieved.

Appendix: Wall-Layer Model

In this Appendix, the embedded functions for the wall-layer profiles of velocity and total enthalpy are summarized[9,10]; these profiles are analytical functions that can easily be evaluated numerically. Both profiles are of the form

$$U^+,\theta^+ = \left[1+(t_0^+/T_B^+)\right]\left[R(T_B^*,t_0^*)Q(\tilde{Y}^+)+Z(\tilde{Y}^+)\right] - (t_0^+/T_B^+)\left[R(0,t_0^+)Q(\tilde{Y}^+)+Z(\tilde{Y}^+)\right] \tag{A1}$$

Here, t_0^+ is a parameter (to be determined) and T_B^+ is the mean period between bursts in the wall layer, having a typical value[10] of $T_B^+ = 110.2$. The functions in Eq. (A1) are given by

$$R(t,t_0^+) = A_0 + \frac{a_0}{4}\log(t+t_0^+) \tag{A2}$$

$$Q(y) = (2y^2+1)\,\mathrm{erf}\,y + \frac{2}{\sqrt{\pi}}\,ye^{-y^2} \tag{A3}$$

$$Z(y) = \frac{2a_0}{\sqrt{\pi}}\left[(2y^2+1)\Xi(y)+y\Xi'(y) - \frac{\sqrt{\pi}}{8}(6y^2+1)\,\mathrm{erf}\,y - \frac{3}{4}\,ye^{-y^2}\right] \tag{A4}$$

Here, a_0 and A_0 are constants whose values are given by

$$a_0 = \frac{2}{\kappa}, \qquad A_0 = C_i - \frac{1}{\kappa}\left[\frac{\gamma_0}{2} - \log 2\right] \tag{A5}$$

for the velocity profiles U^+, where C_i is the inner region log-law constant [c.f., Eq. (19a)], κ is the von Kármán constant, and γ_0 is Euler's constant. For the total enthalpy profile θ^+, replace κ with κ_θ and C_i with B_i in Eq. (A5). For the velocity profile U^+, the variables apearing in Eq. (A1) are

$$\tilde{Y}^+ = Y^+/2\sqrt{T_B^+ + t_0^+}, \qquad \tilde{Y}_0^+ = Y^+/2\sqrt{t_0^+} \tag{A6}$$

whereas for the enthalpy profile θ^+, Y^+ is replaced with $Y^+\sqrt{Pr}$ in Eq. (A6) [c.f., Eq. (19b)]. Finally, the function Ξ is defined by

$$\Xi(y) = \int_0^y e^{-z^2}\int_0^z e^{\xi^2}\int_0^\zeta e^{-x^2}\,d\xi\,dx\,dz \tag{A7}$$

A list of the properties of this function is given in Ref. 26. In particular, it may be shown that

$$\Xi(y) \sim \frac{\sqrt{\pi}}{4}\left\{\log y + \frac{\gamma_0}{2} - \frac{1}{4y^2} + \cdots\right\}, \qquad \text{as } y\to\infty \tag{A8}$$

At the wall, the profile U^+ and θ^+ satisfy Eqs. (24) and (25). For the velocity profile U^+, these conditions require[10] that

$$\sqrt{T_B^+ + t_0^+}\left[R(T_B^+,t_0^+) - \frac{1}{\kappa}\right] - \sqrt{t_0^+}\left[R(0,t_0^+) - \frac{1}{\kappa}\right] = \frac{\sqrt{\pi}}{2}\,T_B^+ \tag{A9}$$

$$(T_B^+ + t_0^+)^{-1/2}R(T_B^+,t_0^+) - (t_0^+)^{-1/2}R(0,t_0^+) = 0 \tag{A10}$$

For the total enthalpy profile, κ_θ replaces κ in Eqs. (A5), (A9), and (A10), and B_i replaces C_i in Eq. (A5); in addition, the right side of Eq. (A9) is multiplied by $\sqrt{Pr}$.

Acknowledgments

The development of the wall-layer velocity profile models was sponsored by the Air Force Office of Scientific Research as part of an investigation of the coherent structure of turbulent boundary layers (Contract F49620-78-C-0071). The heat transfer model development was supported by NASA Ames Research Center (Grant NSG-2135). The investigations described in this paper were sponsored by an independent research program of the United Technologies Research Center. The authors would like to express their appreciation for a number of technical discussions with J. E. Carter and D. E. Edwards of United Technologies Research Center.

References

[1]Fendell, F. E., "Singular Perturbation and Turbulent Shear Flow Near Walls," *Journal of Astronautical Sciences,* Vol. 20, No. 3, 1972, pp. 129–165.

[2]Mellor, G. L., "The Large Reynolds Number Asymptotic Theory of Turbulent Boundary Layers," *International Journal of Engineering Science,* Vol. 10, No. 10, 1972, pp. 851–873.

[3]Melnik, R. E., "Turbulent Interactions on Airfoils at Transonic Speeds—Recent Developments in Computation of Viscous-Inviscid Interactions," AGARD-CP-291, 1980, pp. 10-1–10-34.

[4]Mellor, G. L., and Gibson, D. M., "Equilibrium Turbulent Boundary Layers," *Journal of Fluid Mechanics,* Vol. 24, No. 2, 1966, pp. 225–253.

[5]Cebeci, T., and Smith, A. M. O., *Analysis of Turbulent Boundary Layers,* Academic, New York, 1974.

[6]Edwards, D. E., Carter, J. E., and Werle, M. J., "Analysis of the Boundary Layer Equations Including a New Composite Coordinate Transformation—The ABLE Code," United Technologies Research Center Rept. 81-30, May 1982.

[7]Van Driest, E. R., "On Turbulent Flow Near a Wall," *Journal of Aeronautical Sciences,* Vol. 23, No. 11, 1956, p. 1007.

[8]Cantwell, B. J., "Organized Motion in Turbulent Flow," *Annual Review of Fluid Mechanics,* Vol. 13, 1981, pp. 457–515.

[9]Walker, J. D. A., Scharnhorst, R. K., and Weigand, G. G., "Wall Layer Models for the Calculation of Velocity and Heat Transfer in Turbulent Boundary Layers," AIAA Paper 86-0213, 1986.

[10]Walker, J. D. A., Scharnhorst, R. K., and Weigand, G. G., "A Wall Layer Model for the Velocity Profile in Turbulent Flows," *AIAA Journal,* Vol. 27, No. 2, 1989, pp. 140–149.

[11]Walker, J. D. A., "Wall-Layer Eruptions in Turbulent Flows," *Structure of Turbulence and Drag Reduction,* edited by A. Gyr, Springer-Verlag, New York, 1990, pp. 109–118.

[12]Walker, J. D. A., "Models Based on Dynamical Features of the Wall Layer," *Applied Mechanics Reviews,* Vol. 43, No. 5, Pt. 2, May 1990.

[13]Launder, B. E., and Spaulding, D. B., "The Numerical Computation of Turbulent Flows," *Computer Methods in Applied Mechanics and Engineering,* Vol. 3, 1974, pp. 269–289.

[14]Rubesin, M. R., and Viegas, J. R., "A Critical Examination of the Use of Wall Functions as Boundary Conditions in Aerodynamic Calculations," *Third Symposium on Numerical and Physical Aspects of Aerodynamic Flows,* edited by T. Cebeci, California State University, Long Beach, CA, 1985.

[15]Viegas, J. R., Rubesin, M. W., and Horstmann, C. C., "On the Use of Wall Functions for Two-Dimensional Separated Compressible Flow," AIAA Paper 85-0180, 23rd Aerospace Science Meeting, Reno, NV, Jan. 1985.

[16]Saxena, S. K., and Mehta, R. C., "Shock/Turbulent Boundary-Layer Interaction with Wall Friction Boundary Conditions," *AIAA Journal,* Vol. 24, No. 7, 1986, pp. 1207–1209.

[17]Wahls, R. A., Barnwell, R. W., and DeJarnette, F. R., "A Finite Difference Outer Layer and Integral Inner Layer Method for the Solution of the Turbulent Boundary-Layer Equations," AIAA Paper 87-0429, 25th Aerospace Sciences Meeting, Reno, NV, Jan. 1987.

[18]Walker, J. D. A., Werle, M. J., and Ece, M. C., "An Embedded Function Approach for the Calculation of Turbulent Flow Near Walls," UTRC Report 86-78, March 1987.

[19]Weigand, G. G., "Forced Convection in a Nominally Steady Turbulent Boundary Layer," Ph.D. Dissertation, Purdue Univ., Lafayette, IN, 1978.

[20]He, J., Kazakia, J. Y., and Walker, J. D. A., "Embedded Function Methods for Supersonic Turbulent Boundary Layers," AIAA Paper 90-0306, 28th Aerospace Sciences Meeting, Reno, NV, 1990.

[21]Andersen, P. J., Kays, W. M., and Moffatt, R. J., "The Turbulent Boundary Layer on a Porous Plate: An Experimental Study of the Fluid Mechanics for Adverse-Free-Stream Pressure Gradients," Rept. HMT-15, Dept. of Mechanical Engineering, Stanford Univ., Stanford, CA, 1972.

[22]Blackwell, B. F., Kays, W. M., and Moffatt, R. J., "The Turbulent Boundary Layer on a Porous Plate: An Experimental Study of the Heat Transfer with Adverse Pressure Gradients," Rept. HMT-16, Dept. of Mechanical Engineering, Stanford Univ., Stanford, CA, 1972.

[23]Graziani, R. A., Blair, M. F., Taylor, J. R., and Mayle, R. E., "An Experimental Study of Endwall and Airfoil Surface Heat Transfer in a Large Scale Turbine Blade Cascade," *Journal of Engineering for Power,* Vol. 102, No. 2, 1980, pp. 257–267.

[24]Bachalo, W. D., Modaress, D., and Johnson, D. A., "Experiments on Transonic and Supersonic Turbulent Boundary-Layer Separation," AIAA 15th Aerospace Sciences Meeting, Paper 77-47, 1977.

[25]Degani, A. T., and Walker, J. D. A., "Computation of Three-Dimensional Turbulent Boundary Layers with Heat Transfer in a Plane of Symmetry Using Embedded Wall-Layer Functions," AIAA Paper 90-0307, 28th Aerospace Sciences Meeting, Reno, NV, 1990.

[26]Walker, J. D. A., and Scharnhorst, R. K., "The Ξ Function," Dept. of Mechanical Engineering and Mechianics, Lehigh University, Bethlehem, PA, Rept. FM-90, 1986; Air Force Office of Scientific Research, AFOSR-TR-1715TR (available NTIS-AD-A188680).